Density functional theory study of the electrochemical interface between a Pt electrode and an aqueous electrolyte using an implicit solvent method

Sung Sakong[1],* Maryam Naderian[1], Kiran Mathew[2], Richard G. Hennig[2], and Axel Groß[1,3†]
[1] *Institute of Theoretical Chemistry, Ulm University, 89069 Ulm, Germany*
[2] *Department of Materials Science and Engineering, University of Florida, Gainesville, Florida 32611, USA*
[3] *Helmholtz Institute Ulm (HIU), Electrochemical Energy Storage, 89069 Ulm, Germany*

We present a computational study of the interface of a Pt electrode and an aqueous electrolyte employing semi-empirical dispersion corrections and an implicit solvent model within first-principles calculations. The electrode potential is parametrized within the computational hydrogen electrode scheme. Using one explicit layer, we find that the most realistic interface configuration is a water bilayer in the H-up configuration. Furthermore, we focus on the contribution of the dispersion interaction and the presence of water on H, O and OH adsorption energies. This study demonstrates that the implicit water scheme represents an computationally efficient method to take the presence of an aqueous electrolyte interface with a metal electrode into account.

I. INTRODUCTION

Applying density functional theory (DFT) to electrochemical systems, i.e., developing a seamless atomistic description of the metallic electrode, electrolyte and the interface between electrode and electrolyte from first principles, is a key research tool in the study of electrocatalytic reactions, batteries and fuel cells [1–4]. Unfortunately, many ultra-high vacuum based experimental techniques which have been so successful in the field of surface science cannot be applied to electrochemical systems, in particular if they rely on the diffraction and scattering of electrons. Hence the realistic modeling of electrode-electrolyte interfaces can contribute significantly to obtain a better understanding of the microscopic details of the electrochemical processes. However, in practice, the modeling is hindered by several known obstacles [4–7].

First of all, conventional DFT methods have difficulties to appropriately address the electrode potential, because a practical implementation of the electrode potential within a grand canonical ensemble is missing in electronic structure theories. Besides, the liquid nature of the electrolyte requires a proper thermodynamical sampling which is computationally rather demanding on the basis of ab initio molecular dynamics (AIMD) simulations [3, 4]. Moreover, it is important to take the long range dispersion interaction into account in the description of electrode-electrolyte interfaces [8, 9] as well as the electrolyte [10, 11] which up to recently has usually not been considered within the conventional DFT framework. There are several attempts to address these practical difficulties by, e.g., using a thermodynamical scheme to represent the electrode potential [12–16], employing implicit solvation methods [17–24] and density functionals with van der Waals corrections [10, 25, 26]. In this study, we will apply a combination of these computational schemes in order to address electrochemical electrode-electrolyte interfaces. Firstly, in order to simulate the electrode-electrolyte interface within periodic DFT calculations, the slab approach is employed which is a standard method in surface science, i.e., surfaces are represented by a periodic array of slabs separated by a sufficiently large vacuum layer. In electrochemical problems, the vacuum should be filled with solvent molecules. As far as aqueous electrolytes are concerned, the water molecules at the interface are typically modeled by hexagonal a water bilayer of coverage of 2/3 that is found in ultra high vacuum experiments [27, 28]. Of course, the ground state configurations of water molecules in crystalized networks differ from those in liquid phase. Therefore, the liquid molecules should be explicitly simulated by thermodynamic sampling methods. Using this technique, it has been shown that water layers at close-packed metal electrode surfaces are indeed not crystalline [29]. However, because of the high computational demand associated with AIMD simulations, there is an attempt to employ numerically efficient solvation methods to simulate the liquid molecules at the interface [30].

Solvation methods correspond to a system-bath model, i.e., the system part includes the electrode and molecules at the interface and the bath consists of liquid water at a specific thermodynamic condition. The coupling between system and bath is described through the solvation energy, and the bath changes the electrostatic potential in the system part. The idea is based on the assumption that the atoms of the electrode and the molecules at the interface are more ordered than in molecules in the liquid phase. Thus, the degrees of freedom of the electrode atoms and molecules at the interface can be decoupled to a certain degree from those of the molecules in the electrolyte. Faheem and Heyden introduced a reservoir described by molecular mechanics using classical force field methods [30]. Within the solvation method approach, the bath can be further simplified by employing a dielectric continuum method in the so-called implicit solvent method [17–24, 31–33]. In this approach, the liquid

* sung.sakong@uni-ulm.de
† axel.gross@uni-ulm.de

reservoir is described by a dielectric medium, and the solvation energy of the system is a function of the relative permittivity that depends on the charge density of the system part. Of course, within this approach it is not necessary to take any solvent molecules explicitly into account [33].

Another technical issue is the consideration of the long range dispersion interaction within conventional DFT framework in order to describe liquid properties and electrode-electrolyte interfaces more appropriately. There is a parameter free method to account for electron correlations with dispersion interactions [34], but the computational demand for this approach had been significantly higher compared to conventional DFT. Therefore, several efficient semi-empirical schemes have been proposed to correct the correlation energies and corresponding forces using pairwise potentials, so-called vdW-D methods [26, 35]. Alternately, Dion et. al. proposed a non-local correlation functional with approximated dispersion interactions (vdW-DF) [36]. Furthermore, Wellendorff et al. recently introduced a new exchange-correlation functional (Bayesian error estimation functional: BEEF) which is optimized together with vdW-DF to reference systems for catalytic reactions [37].

Last but not least, in order to take varying electrode potentials into account Nørskov introduced the concept of the computational hydrogen electrode [12–16]. It is based on the fact that at standard conditions of 1 atm and 298.15 K the proton H^+ in solution is at equilibrium with the H_2 molecule in gas phase.

$$2H^+(aq) + 2e \rightleftharpoons H_2(g). \quad (1)$$

This avoids to derive solvation energies which can be computationally rather demanding. Furthermore, it is well-known how the chemical potential of the proton in solution changes as a function of the absolute electrode potential U^{abs} compared to an electron in vacuum by

$$\tilde{\mu}_H(U^{abs}) = \mu_{H^+(aq)} + \mu_e = \mu_{H^+(aq)} - eU^{abs}. \quad (2)$$

The corresponding electrode potential is denoted as the standard hydrogen electrode (SHE) and the potential (U_{SHE}) is at approximately 4.3 V compared to the vacuum level [38, 39]. Then, the μ_{H^+} can be expressed in terms of the energy of the hydrogen gas at standard conditions. Conventionally, the electrode potential is expressed with respect to U_{SHE}.

Then, the chemical potential of hydrogen at the electrode potential U can be written as

$$\tilde{\mu}_H(U) = \mu_{H^+(aq)} - e(U + U_{SHE}) = \frac{1}{2}E_{H_2(g)} - eU. \quad (3)$$

Furthermore, the concentration of the protons enters the chemical potential through the additional term $k_B TpH$.

In this study, we combine the three approaches to address electrochemical interface between a Pt electrode and an aqueous electrolyte. We evaluate the adsorption energies of hydrogen, oxygen and hydroxyl as a function of the coverage and the electrode potential in an aqueous environment for different functionals. The results using the implicit solvent model will be compared to those obtained with an explicit water bilayer.

II. NUMERICAL METHODS

The total energies of the systems have been calculated using the periodic DFT code *Vienna ab initio simulation package* VASP [40]. The wave functions have been expanded in a plane wave basis set with an energy cutoff of up to 700 eV. The electronic cores are described by the projector augmented wave method [41]. The exchange-correlation energies have been evaluated within the generalized gradient approximation (GGA). We employ GGA functionals as suggested by Perdew, Burke and Ernzerhof (PBE) [42], by Hammer and Nørskov (RPBE) and by Wellendorff et. al. (BEEF) [37]. Dispersion interactions have been taken into account using semi-empirical corrections (vdW-D) as proposed by Tkatchenko and Scheffler (TS) [26] and by Grimme et. al. (D3) [25]. In BEEF functional, the dispersions interactions are evaluated using the Langreth and Lundqvist's vdW-DF2 scheme [36] as implemented by Klimeš et. al. [10, 43]. We will compare the performance of the PBE, PBE-D3, PBE-TS, RPBE, RPBE-D3 and BEEF functionals in the description of the interface between an aqueous electrolyte and a Pt electrode.

The optimized lattice constants of fcc Pt are 3.94, 3.93, 3.97, 3.99, 3.78 and 3.99 Å for the PBE, PBE-D3, PBE-TS, RPBE, RPBE-D3 and PBE-TS functionals, respectively. The calculations agree with the experimental value of 3.92 Å with smaller error than 2%, except for the RPBE-D3 functional which leads to a relatively large underestimation of the Pt lattice constant by 3.5 %. The Pt electrode is modeled by a Pt(111) slab with five atomic layers. The top three layers are fully relaxed, while the two bottom layers are fixed at their bulk positions. The slab is separated by a vacuum of 15 Å to avoid the interaction between the periodic images of the slab. A 3×3 surface unit cell has been selected in the calculations, and a $5 \times 5 \times 1$ k-point grid has been used in the k-point sampling of the first Brillouin zone.

In order to discuss atomistic details of the water-electrode interface, we insert an explicit hexagonal water bilayer on the Pt surface within the $\sqrt{3} \times \sqrt{3}$ geometry, ice-like layers in the so-called H-down and H-up configurations with a coverage of 2/3 [6, 8, 15, 29]. In these bilayers, every second adsorbed water molecule is oriented parallel to the surface while the other water molecules have one H atom either pointing up or down with respect to the water layer. Furthermore, we also considered explicit water coverages of 1/9, 2/9 and 1/3 with/without implicit solvent in order to assess the influence of the explicit water molecules on the properties of the electrode/electrolyte interface.

The solvation energies in implicit water are evalu-

ated within the joint density functional theory framework [17, 19, 20, 22] as implemented into VASP by Mathew and Hennig [24]. The background dielectric constant of water is $\epsilon_b = 80$ and the cutoff charge density is $\rho_{\rm cut} = 0.0025\,\text{Å}^{-3}$. The cavitation energies are calculated with a surface tension parameter of $0.525\,\text{meV/Å}^2$ [23] as described in Ref. 33.

III. STANDARD ELECTRODE POTENTIALS

In order to demonstrate the computational hydrogen electrode approach, standard electrode potentials have been evaluated by determining the energy difference between reactants and products of redox couples in an aqueous environment. Practically, the required information corresponds to the atomization energy and solvation free energy of the involved molecules. We note that the energies can be determined experimentally or numerically. For those electrode potentials that are determined by the experimental atomization energies of gaseous molecules, the values are taken from the Computational Chemistry Comparison and Benchmark DataBase (CCCBDB) [44]. Since experimental solvation free energies are not available for all involved molecules in the considered electrochemical reactions, we estimate the solvation energies numerically. As shown in Table I, the implicit solvation method effectively reproduces available experimental values. Furthermore, the solvation energy of a water molecule in implicit water is in the range of 0.30–0.32 eV for the six density functionals considered in this study. Thus the difference between the considered density functionals is relatively small. Therefore, we will use the solvation energies calculated by PBE-TS functional to determine the energies of aqueous molecules.

We selected several electrochemical reactions in acidic solutions (pH = 0) from a data base [45] with the proton being the only ion in the reaction so that the electrode potentials can be related to the standard hydrogen electrode using Eq. 3. Thus the calculation of charged species can be avoided which is problematic within a periodic DFT setup [29]. The considered reactions are listed in Table II. We will illustrate the computational scheme to derive the standard electrode potentials using the reaction

$$\frac{1}{2}\mathrm{O_2(g)} + 2\mathrm{H^+(aq)} + 2e \rightarrow \mathrm{H_2O(aq)} \qquad (4)$$

as an example. The measured electrode potential is $U = 1.2291\,\text{V}$ [45]. The energy of $\mathrm{H^+(aq)}$ has been related to $\mathrm{H_2(g)}$ according to Eq. 3. Thus a standard electrode potential of $U = 1.40\,\text{V}$ has been evaluated for this reaction using experimental atomization energies. We note that the entropic contributions for the gaseous species is negligible, for example, the thermal entropy of $\mathrm{H_2}$ gas at standard conditions (298 K and 1 atm) is only 2 meV based on ideal gas theory [46], in good agreement with the experimental estimate of 1 meV [47]. Thus we will neglect the entropic contributions in the evaluation of electrode potentials.

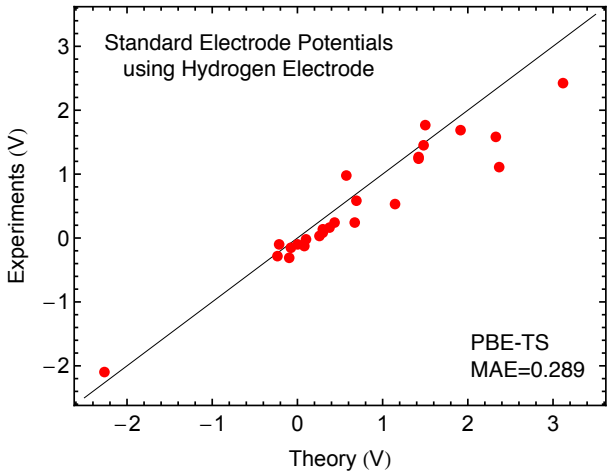

FIG. 1. Comparison between theoretical and experimentally measured standard electrode potentials of various electrochemical reactions. The potentials are in Volt. The blue squares, red circles and green triangles represent theoretical calculations using experimental values, PBE-TS calculations and CCSD(T) calculations, respectively.

In Fig. 1, the calculated electrode potentials of the electrochemical reactions listed in Table II are compared to the experimental half cell potentials. The electrode potentials are evaluated using solvation energies from PBE-TS calculations and atomization energies from experiments (depicted in squares), highly accurate coupled cluster calculations (depicted in triangles) and PBE-TS calculations (depicted in circles). The values of the coupled cluster calculations (CCSD(T) with aug-cc-pVTZ basis) are taken from CCCBDB [44].

There is a satisfactory linear correlation between calculated and measured values. Using experimental at-

TABLE I. Solvation energies of selected molecules in implicit solvent are presented in eV. The negative sign means an energy gain by solvation of a molecule. The experimental values are from a) Ref. 48 and b) Ref. 49.

Molecule	Experiments	PBE-TS
$\mathrm{H_2O}$	$-0.27^{a)}$	−0.31
$\mathrm{CH_3OH}$	$-0.21^{a)}$, $-0.54^{b)}$	−0.20
$\mathrm{HCHO_2}$	$-0.24^{a)}$	−0.34
$\mathrm{CH_2O}$		−0.17
$\mathrm{CO_2}$	$-0.19^{b)}$	−0.11
$\mathrm{CH_4}$	0.09, $-0.12^{b)}$	0.02
$\mathrm{HNO_2}$		−0.00
$\mathrm{O_2}$	$-0.01^{b)}$	0.02
$\mathrm{H_2}$	$-0.00^{b)}$	0.01

omization energies, the computational hydrogen electrode method reproduces the experimental half cell potentials with a relatively small mean absolute error of 0.13 V. Hence, the electrode potentials can be effectively estimated by the computational hydrogen electrode method. However, we note that several calculated potentials can be off by more than 0.2 V, for example in the NO(g),H^+/N_2O(g) and O(g),H^+/H_2O(aq) couples. This might imply that the expression of the reactions may be incomplete, i.e., other ions rather than H^+ can be involved in the half cell reaction.

When numerically evaluated atomization energies are used, the mean absolute error becomes 0.29 and 0.21 V for PBE-TS and CCSD(T) calculations, respectively.

TABLE II. Standard electrode potentials of electrochemical reactions calculated using (i) experimental values, (ii) PBE-TS calculations and (iii) CCSD(T) calculations. We note the mean absolute errors are 0.13, 0.29 and 0.21 V for the selected reactions, when the atomization energies from experiment, PBE-TS calculations, and CCSD(T) calculations are used. We calculated the energies of molecules in aqueous state by means of the implicit solvent model. The crystal of C, Si and Ge is assumed in the diamond structure.

	$U_{exp.}$	$U_{calc.}$ (V)		
Reactions		(i)	(ii)	(iii)
H^+/H(g)	−2.107	−2.26	−2.27	−2.35
C(c),H^+/CH_3OH(aq)	−0.320		−0.09	
Ge(c),H^+/GeH_4(g)	−0.294		−0.24	
Si(c),H^+/SiH_4(g)	−0.147		−0.08	
CO_2(g),H^+/$HCHO_2$(aq)	−0.114	−0.02	0.08	0.23
CO_2(g),H^+/CO(g)	−0.104	−0.08	−0.21	0.02
H^+/H_2(aq)	−0.091	−0.01	−0.00	0.02
$HCHO_2$(aq),H^+/CH_2O(aq)	−0.029	−0.06	0.09	−0.02
CH_3OH(aq)/CO_2(aq),H^+	0.020	0.12	0.26	0.27
C(c),H^+/CH_4(aq)	0.089		0.30	
C(c),4H^+/CH_4(g)	0.132		0.30	
CO_2(g),H^+/CH_4(g)	0.169	0.28	0.38	0.39
CO_2(aq),H^+/C(c)	0.229		0.44	
CH_2O(aq),H^+/CH_3OH(aq)	0.237	0.44	0.67	0.65
CO(g),H^+/C(c)	0.528		1.14	
CH_3OH(aq),H^+/CH_4(g)	0.583	0.66	0.69	0.69
HNO_2(aq),H^+/NO(g)	0.984	1.12	0.58	
NO_2(g),H^+/HNO_2(aq)	1.108	1.13	2.38	
O_2(g),H^+/H_2O(aq)	1.229	1.39	1.42	1.49
O_2(aq),H^+/H_2O(aq)	1.272	1.42	1.42	1.49
HNO_2(aq),H^+/N_2(g)	1.447	1.62	1.47	
NO(g),H^+/N_2O(g)	1.587	1.91	2.33	
NO(g),H^+/N_2(g)	1.678	1.85	1.92	
N_2O(g),H^+/N_2(g)	1.769	1.79	1.50	1.91
O(g),H^+/H_2O(aq)	2.430	2.68	3.13	2.73
Mean Absolute Error		0.13	0.29	0.21

Since in all reactions listed in Table II either H_2(g) or H_2O(g) or both are involved, the accuracy of the atomization energies of the molecules influences the overall DFT results. PBE-TS and CCSD(T) estimate the H_2 binding energy to be 4.54 and 4.71 eV, respectively, which should be compared with the experimental value of 4.52 eV. In the reactions involving H^+/H(g), PBE-TS reproduces the experiments better than CCSD(T). However, as far as the atomization energy of H_2O(g) is concerned, CCSD(T) (9.90 eV) reproduces the experimental value of 9.96 eV better than PBE-TS (10.48 eV).

Thus PBE-TS leads to a relatively large absolute error, in particular for the gaseous oxygen atom (O(g),H^+/H_2O(aq) reaction), because the binding energy of the O-H bond is overestimated. This will lead to calculated potentials that are systematically larger than the measured ones, in fact for all three methods. Sometimes the error is canceled, for example by the well-known problem of GGA functionals to reproduce the O_2 binding energy. Consequently, PBE-TS predicts the reaction of O_2(g),H^+/H_2O(aq) correctly, because the error in O-H bond formation is compensated by the error for O-O bond breaking. Therefore, using numerical methods, the computational hydrogen electrode method reproduces electrode potentials with a relatively large mean absolute error of 0.2-0.3 V. The error depends on the accuracy of the atomization energies of involved molecules in the electrochemical reactions and, thus, the error is not systematically controllable.

However, for many other reactions, the error is below 0.2 V which is certainly acceptable regarding the approximations entering the evaluation of the standard electrode potentials. Therefore, we conclude that the combination of the computational hydrogen electrode together with the implicit solvent method is applicable to describe electrochemical systems involving coupled proton-electrode charge transfer, but this approach still suffers from the well-known problems of conventional DFT calculations for chemical reactions.

IV. Pt ELECTRODE-WATER INTERFACE

In this section, we address the interface between a Pt(111) electrode and water. As mentioned in the introduction, AIMD simulations have already shown that water layers at room temperature are disordered, at least as far as the orientation of the water molecules is concerned [29, 50]. However, we are rather concerned with the performance of different density functionals and the implicit solvent model in the description of interfaces. The configurations of explicit water molecules at the interface studied in our work are illustrated in Fig. 2. Isolated water molecules are considered in a hexagonal arrangement at coverage of 1/9, 2/9 and 1/3 (see Fig. 2a-c). Water networks at the interface are modeled by a dimer (Fig. 2d) and hexagonal ice-like H-down (Fig. 2e) and H-up structures (Fig. 2f).

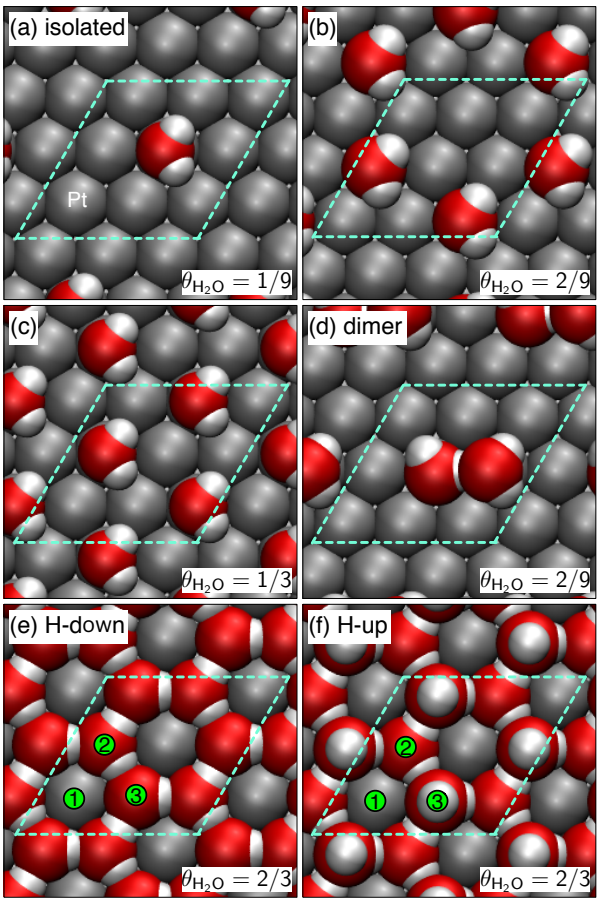

FIG. 2. Top view of various explicit water configurations on Pt(111) considered in this study with coverages between 1/9 and 2/3.

The formation enthalpies of the water structures on the Pt electrode are determined with respect to the Pt slab and a single water molecule in the gas and in the liquid phase by performing calculations without and with implicit water:

$$E_f = (E_{H_2O/Pt(111)} - E_{Pt(111)} + nE_{H_2O})/n. \quad (5)$$

Here, $E_{H_2O/Pt(111)}$, $E_{Pt(111)}$ and E_{H_2O} are the total energies of the whole system, the isolated metal slab and the water molecule in vacuum and in implicit water, respectively. n represents the number of water molecules per cell. We assume that the Pt slab in the presence of implicit water is a thermodynamic equilibrium configuration between the electrode and electrolyte. Then, the formation enthalpy in vacuum corresponds to the adsorption energy of the water structure, whereas the formation enthalpy in implicit water corresponds to an energy gain of a specific atomistic configuration compared to the thermal average of liquid water. The assumption requires that the averaged formation enthalpy of all explicit water configurations vanishes after an extensive thermodynamic sampling in the presence of an implicit solvent. In this study, we cannot prove this assumption, but we will adopt the literal definition of the formation enthalpy.

As we discussed in previous work [3], there are two contributions to the formation enthalpy of water structures or networks (dimer or water bilayers); the network formation and the adsorption of a water molecule which can also be described as the water-water and the water-metal interaction. These two contributions cannot be uniquely separated [51]. Here we estimate them by defining two different reference configurations.

Comparing the adsorption energy of the total water structure with the one of an isolated water molecule (see Fig. 2a) leads to an estimate for the network formation energy E_{net}:

$$E_{net} = (E_{H_2O/Pt(111)} - E_{Pt(111)} + nE_f[H_2O])/n, \quad (6)$$

with $E_f[H_2O]$ being the formation enthalpy of a single water molecule on the surface. On the other hand, comparing the adsorption energy of the total water structure with the energy of an isolated water network in the gas phase E_{nH_2O} yields an estimate for the adsorption energy E_{ads} with respect to the water network

$$E_{ads} = (E_{H_2O/Pt(111)} - E_{Pt(111)} + E_{nH_2O})/n. \quad (7)$$

First we address the dimer formation energy in gas phase. A water dimer is mainly bound through a hydrogen bond. The corresponding formation enthalpy is -0.2177 eV according to highly accurate coupled cluster calculations [52]. In contrast, conventional GGA functionals lead to a deviation of the dimer formation enthalpy from the coupled cluster results by -0.02 eV for PBE and 0.05 eV for RPBE. PBE accurately yields the dimer formation enthalpy in spite of the lack of dispersion interactions which is crucial in noncovalent bonds [11]. It is a known problem that the PBE functional reproduces the water-water interaction correctly because of the wrong reasons [3, 8, 11]. Including vdW-D corrections, the formation enthalpies differ from the coupled cluster results by -0.03 eV (PBE-D3), -0.02 eV (PBE-TS), and 0.00 eV (RPBE-D3), respectively.

The vdW-D corrections increase the discrepancy in the water formation enthalpy with respect to the coupled cluster results for the PBE functional whereas they reduce it for the RPBE functional. Furthermore, vdW-D corrections are smaller for the PBE functional than for the RPBE functional. As far as the properties of liquid water is concerned, the vdW-D contribution does not correct [11] the well-known overstructuring of liquid water in PBE functional [53–55]. For RPBE-D3, the overestimated directional hydrogen bonding of the PBE functional is replaced by the non-directional van der Waals interaction. Consequently, the RPBE-D3 functional reproduces liquid water properties such as pair distribution functions at room temperature rather well [11]. Summarizing these findings, all dispersion corrected functionals describe the energetics of the water-water interaction sat-

isfactorily, but only the RPBE-D3 also reproduces the structural properties of liquid water well.

Turning now to the water structures on Pt(111), we have collected in Table III the formation enthalpy, adsorption energy and network formation energy of the water structures depicted in Fig. 2 at the electrode-vacuum and the electrode-implicit water interfaces for the considered density functionals. Note that our PBE results agree well with previously calculated values [56, 57]. The pure water-Pt interaction can be derived from the water adsorption energy at a coverage of $\theta_{H_2O} = 1/9$ in vacuum, because the water-water interaction should be minimal in this configuration. While the energetics of the hydrogen bond are rather similar for all considered functionals reflected by the similar values for the water dimer formation energy, the strength of the Pt-water interaction varies noticeably among these functionals. For RPBE, the adsorption energy of 0.08 eV indicates a rather weak interaction. For PBE and BEEF, comparable adsorption energies of about 0.3 eV result. Upon including semi-empirical dispersion corrections (vdW-D), the binding energy of the water molecule to Pt(111) increases to a range between 0.5 and 0.6 eV. Note that there is a more significant vdW-D correction for RPBE-D3 than for PBE-D3 and PBE-TS, i.e., a stronger dispersion interaction between water and Pt is predicted for RPBE-D3. As a result, the binding energy is 0.1 eV larger for RPBE-D3 than for PBE-D3 and PBE-TS.

The formation enthalpy per water molecule decreases slightly with increasing coverage of still isolated water molecules (Fig. 2a to c) for all density functionals and both considered environments. With increasing coverage, the distance between the single water molecules decreases and apparently the repulsive dipole interaction between water molecules increases. As indicated by a spectroscopy experiment by Ogasawara et. al. [58], water monomers can only exist at low water coverage and low temperature, e.g., below 40 K. However, we are not aware of any experiments yielding the adsorption energy of isolated water molecules on Pt(111). Hence the calculated DFT values can not be validated by any measurements.

At the electrode-vacuum interface, the water dimer formation on Pt surface (configuration Fig. 2d) is energetically more favorable than the adsorption of single water molecules by about 0.1 eV per water molecule for all considered functionals (see Table III) due to the additional energy gain upon the formation of the hydrogen bond between the two water molecules. As discussed above, a quantitative separation of the formation energy into contributions from the water-water and the water-metal interaction is not uniquely possible. We note that the averaged adsorption energy E_{ads} determined according to Eq. 7 for the water dimer is comparable with the the one of an isolated water molecules, whereas the dimerization energy E_{net} according to Eq. 6 is around 0.1 eV smaller on the surface than in the gas phase. This indicates that the water-water interaction in the dimer is weakened on the surface, but it is still strong enough that water cluster

TABLE III. Formation enthalpy E_f and adsorption energies with respect to a free standing water layer E_{ads} and with respect to an isolated adsorbed water molecule E_{net} of the water structures depicted in Fig. 2 on Pt(111) surface in vacuum or in implicit water. Note that for the adsorbed structures in the presence of implicit water, the energy reference is also taken in implicit water.

		vacuum (eV)			implicit water (eV)		
PBE	θ_{H_2O}	E_f	E_{ads}	E_{net}	E_f	E_{ads}	E_{net}
(a)	1/9	−0.29	-	-	−0.37	-	-
(b)	2/9	−0.25	-	-	−0.27	-	-
(c)	1/3	−0.23	-	-	−0.19	-	-
(d)	2/9	−0.42	−0.30	−0.13	−0.33	−0.25	0.05
(e)	2/3	−0.50	−0.05	−0.21	unstable	-	-
(f)	2/3	−0.47	−0.03	−0.19	−0.29	−0.07	0.09
PBE-D3	θ_{H_2O}	E_f	E_{ads}	E_{net}	E_f	E_{ads}	E_{net}
(a)	1/9	−0.52	-	-	−0.58	-	-
(b)	2/9	−0.49	-	-	−0.48	-	-
(c)	1/3	−0.47	-	-	−0.40	-	-
(d)	2/9	−0.63	−0.50	−0.11	−0.51	−0.43	0.07
(e)	2/3	−0.72	−0.23	−0.20	unstable	-	-
(f)	2/3	−0.67	−0.18	−0.15	−0.50	−0.24	0.08
PBE-TS	θ_{H_2O}	E_f	E_{ads}	E_{net}	E_f	E_{ads}	E_{net}
(a)	1/9	−0.49	-	-	−0.59	-	-
(b)	2/9	−0.45	-	-	−0.48	-	-
(c)	1/3	−0.43	-	-	−0.39	-	-
(d)	2/9	−0.60	−0.48	−0.12	−0.51	−0.43	0.08
(e)	2/3	−0.70	−0.22	−0.21	unstable	-	-
(f)	2/3	−0.65	−0.18	−0.17	−0.49	−0.23	0.10
RPBE	θ_{H_2O}	E_f	E_{ads}	E_{net}	E_f	E_{ads}	E_{net}
(a)	1/9	−0.08	-	-	−0.13	-	-
(b)	2/9	−0.06	-	-	−0.05	-	-
(c)	1/3	−0.06	-	-	0.01	-	-
(d)	2/9	−0.21	−0.13	−0.13	−0.13	−0.10	0.00
(e)	2/3	−0.34	−0.01	−0.27	−0.09	0.03	0.04
(f)	2/3	−0.34	−0.01	−0.26	−0.09	0.03	0.04
RPBE-D3	θ_{H_2O}	E_f	E_{ads}	E_{net}	E_f	E_{ads}	E_{net}
(a)	1/9	−0.60	-	-	−0.57	-	-
(b)	2/9	−0.60	-	-	−0.50	-	-
(c)	1/3	−0.59	-	-	−0.45	-	-
(d)	2/9	−0.69	−0.58	−0.09	−0.46	−0.23	0.11
(e)	2/3	−0.73	−0.30	−0.13	−0.46	−0.23	0.11
(f)	2/3	−0.67	−0.24	−0.07	−0.51	−0.28	0.06
BEEF	θ_{H_2O}	E_f	E_{ads}	E_{net}	E_f	E_{ads}	E_{net}
(a)	1/9	−0.27	-	-	−0.31	-	-
(b)	2/9	−0.26	-	-	−0.25	-	-
(c)	1/3	−0.25	-	-	−0.19	-	-
(d)	2/9	−0.38	−0.28	−0.11	−0.29	−0.23	0.03
(e)	2/3	−0.49	−0.10	−0.21	−0.20	−0.02	0.12
(f)	2/3	−0.49	−0.11	−0.22	−0.29	−0.12	0.02

formations occurs at low coverages, as found in the experiment [58–60] and in AIMD simulations [3]. Because of the stronger Pt-water interactions in the vdW-D methods, the adsorption energy of a water dimer is considerably increased upon inclusion of dispersion corrections, whereas the BEEF functional reproduces the results of PBE functional.

Upon further water adsorption, a complete water network in the form of a bilayer is formed. There are two possible configurations: an H-down (Fig. 2e) and an H-up (Fig. 2f) structure consistent with LEED and spectroscopy experiments [27, 61]. Despite of counter arguments raised by Hodgson and Haq [28], we suppose that bilayer structures are the best theoretical model to simulate a closely packed water structure on metal surfaces at low temperatures. Therefore, we stick to the bilayer scheme when comparing our results to findings of low temperature experiments [62, 63]. Note however, that at room temperature, according to AIMD simulations it is rather likely that the water bilayers on Pt(111) become disordered [29].

In the two dimensional water network, the contribution of the water-water interaction to the formation energy becomes more significant compared to the dimer on the surface, while the contribution of the water-Pt interaction becomes weaker. This is not too surprising considering the fact that in the 2D network every water molecule forms two hydrogen bonds with neighboring water molecules.

For the RPBE functional, the water layers in both the H-down and the H-up configurations do not really bind to Pt(111), as reflected by the negligible adsorption energy of $E_{ads} = -0.01\,\text{eV}$. The bilayers become situated around 5 Å above the surface, because of severely underestimated Pt-water interaction [8]. For the other functionals, the energy minimum structures of the water bilayers are located around 3 Å above the Pt surface. We note that the formation enthalpy of the bilayer structures is the largest in vacuum and the H-down configuration is slightly favored by up to $60\,\text{meV}/\text{H}_2\text{O}$ compared to the H-up configuration. For the BEEF functional, the two configurations are energetically degenerate.

In order to discuss the performance of the considered functionals, we compare the formation enthalpies of the H-down and H-up bilayer structures with experimental values [62, 63]. According to microcalorimetry experiments by the Campbell group performed at 88 K [63], the heat of adsorption of water is 0.56 eV, practically independent from the water coverage up to a coverage of 2/3. When the heat of adsorption is extrapolated to zero Kelvin using the heat capacity of water bilayers [63], it becomes 0.7 eV which compares well with the calculated formation enthalpy for the H-down configuration (Fig. 2e) using the vdW-D methods. For PBE and BEEF, the formation enthalpy is about 0.2 eV smaller than in the experiment. Table III) indicates that the additional stabilization of the vdW-D functionals is caused by the enhanced Pt-water interaction.

Comparing the adsorption energy of a single water molecule in the configuration of Fig. 2a and the cohesive energy of the water dimer in gas-phase, we note that the vdW-D methods yield a Pt-water interaction that is stronger than the water-water interaction. Actually, this result is consistent with the observation in the microcalorimetry experiments [63] that the heat of adsorption becomes smaller for more than two bilayers.

As discussed above, metal-water and water-water interaction compete with each other. Note that both PBE-D3 and PBE-TS yield similar values for the adsorption energy E_{ads} and the network formation energy E_{net}, whereas RPBE-D3 predicts a stronger adsorption energy than network formation energy. Note that the PBE functional leads to an over-structuring of water both without and with dispersion corrections [11, 53–55]. In contrast, the RPBE-D3 functional yields a correct liquid water structure [11] despite of a formation enthalpy that is similar to those of the PBE-D3 and PBE-TS functional.

In implicit water, the formation enthalpy of explicit water molecules at the electrode surface should be zero in an ideal thermal equilibrium with liquid water. Therefore, energetically favorable configurations with formation energies less than 0 eV should be interpreted as a thermodynamic non-equilibrium structure at the liquid water/electrode interface. Of course, as mentioned above, we have not precisely defined the equilibrium energy, but we will use as a reference a Pt slab in the presence of implicit water for the sake of convenience. We note that using this reference, all considered explicit water configurations lead to an energy gain compared to the thermodynamic equilibrium for all methods that we used. In particular, the adsorption of a single water molecule yields a large energy gain, and consequently, the two-dimensional network formation on Pt(111) becomes endothermic.

Interestingly, we find that the H-down configuration becomes unstable in the presence of implicit water when the PBE, PBE-D3, PBE-TS and RPBE functionals are employed. The water bilayer is pushed toward the metal surface in the presence of the implicit solvent by up to 0.5 Å compared to the configuration in vacuum. This causes an increased repulsive interaction between the downward-oriented hydroxyl group and the metal slab. The additional repulsion vanishes upon rotating the water molecule to the H-up configuration. Precisely, the down-oriented hydroxyl group turns parallel to the surface, while the parallel hydroxyl group becomes upward-oriented when the H-down structure is allowed to relax. For the RPBE-D3 and BEEF functionals, the H-down configuration is stable in the presence of the implicit solvent, but the formation enthalpy is smaller than the one for the H-up configuration, contrary to the results in vacuum.

In Fig. 3, the averaged local permittivity and explicit charge densities are depicted with/without H-up bilayer. The local permittivity is calculated as explained in Ref. 24. We note that the local permittivity on bare

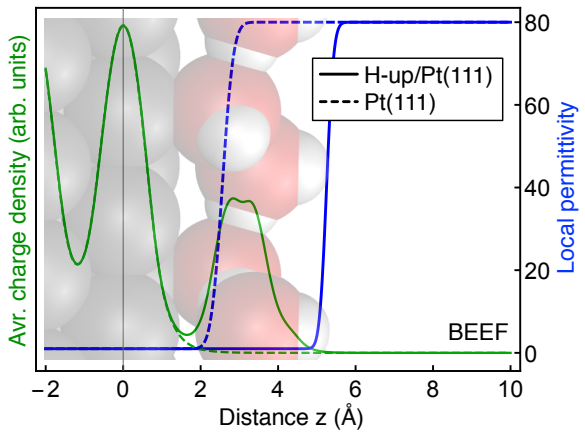

FIG. 3. The charge density and corresponding local permittivity on Pt(111) slab are presented with/without H-up bilayer in a function of the distance from the upper most Pt layer z. The dashed and solid lines are for bare Pt(111) and H-up/Pt(111) calculations, respectively.

Pt(111) (dashed blue line) raises to the level of liquid water at about 3 Å above the surface. As shown in Fig. 3, this corresponds to the position of the first layer of explicit water molecules on Pt(111) in the H-up configuration. Therefore we will use the H-up configuration as the structure for the explicit water layer.

With respect to the electrochemical interface between an aqueous electrolyte and Pt(111) it has to be noted that at low electrode potentials Pt(111) is hydrogen-covered whereas at high electrode potentials Pt(111) becomes OH-covered. In the following, we will therefore consider the adsorption of H and OH in an aqueous environment on Pt(111). The presence of water will be modeled by implicit water and by a combination of one explicit water layer together with implicit water.

V. ADSORPTION OF H, O AND OH AT THE Pt(111)/IMPLICIT WATER INTERFACE

In this section, we determine the adsorption enthalpies of H, O and OH in the presence of an implicit water model as a function of the electrode potential and contrast them with the corresponding enthalpies at the Pt(111)/vacuum interface. The adsorption enthalpy is defined by

$$\Delta H(U) = (E_{tot} - E_{slab} - n_{\mathrm{H}}\tilde{\mu}_{\mathrm{H}}(U) - n_{\mathrm{O}}\mu_{\mathrm{O}})/A \quad (8)$$

where A is area of the unit cell, μ the chemical potential and n the number of ions per unit cell. E_{tot} and E_{slab} are the energies of the Pt electrode with and without adsorbates, respectively. The chemical potential of hydrogen μ_{H} at an electrode potential U is defined by Eq. 3 within the concept of the computational hydrogen electrode. The electrochemical potential of oxygen $\tilde{\mu}_{\mathrm{O}}$ is derived from its equilibrium with a water molecule in the liquid phase, i.e., $\mu_{\mathrm{O}} = E_{\mathrm{H_2O(aq)}} - 2\tilde{\mu}_{\mathrm{H}}$. This avoids the well-known problems of GGA functionals with the O_2 binding energy. Note that the slab energies are calculated separately in vacuum and in implicit water in order to determine the appropriate reference energies.

In Table IV, the adsorption properties of H, O and OH on Pt(111) and their change upon introducing the implicit solvent model are listed. The functionals PBE, PBE-TS, RPBE-D3 and BEEF all yield consistent results. As the RPBE-D3 functional performs best in the description of the water properties, we will in the following focus on this functional.

As far as hydrogen adsorption is concerned, the adsorption enthalpies are practically the same with and without the implicit solvent. These results can be explained by the small Wigner-Seitz radius and the small adsorption height of hydrogen. Therefore, hydrogen adsorption only leads to a modest change in the charge density of the Pt surface which then results only in a small change in the cavitation energy in implicit solvent. This means the energetics of hydrogen adsorption on Pt(111) will hardly be influenced by the inclusion of an implicit solvent.

Our calculations reproduce the peculiarity of Pt(111), namely that there is a small corrugation in the hydrogen adsorption energies. The RPBE-D3 calculations reproduce the results of previous PBE calculations, i.e., the top site is the most favorable adsorption site for hydrogen adsorption at low coverages [6]. However, for higher coverages PBE calculations yield that the fcc hollow site is energetically more favorable [6, 64, 65]. Interestingly enough, RPBE-D3 predicts in contrast to PBE that the top site remains to be the most stable adsorption site also at higher coverages.

The influence of the implicit solvent is more noticeable for larger adsorbates. For example, oxygen adsorption at the top site with an adsorption height of about 2 Å is stabilized by 0.1 eV in the presence of implicit water. For the three-fold hollow adsorption sites, however, the presence of the implicit solvent hardly changes the oxygen adsorption energies. This is different in the case of OH adsorption where on all considered adsorption sites an additional energy gain of about 0.1 eV because of the presence of implicit water. Note that hydrogen adsorption at zero potential is exothermic on all high symmetric sites, whereas O and OH adsorptions are endothermic if liquid water is used as the reservoir for oxygen.

In Fig. 4, the RPBE-D3 formation enthalpies of H, O and OH are displayed as a function of the electrode potential for a variety of coverages. The calculations reproduce the well-known coverage of Pt(111) as a function of the electrode potential [66] almost quantitatively: at low potentials up to about 0.5 V Pt(111) is covered by so-called *upd* hydrogen at monolayer coverage, where *upd* stands for underpotential deposition. This is followed by the double layer region without any particular adsorbate, and at about 0.6 V OH adsorption starts. If oxygen is present, it would form an adsorbate layer at even higher

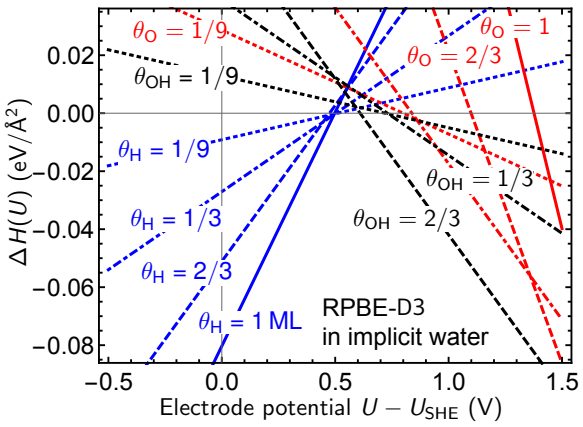

FIG. 4. Formation enthalpies of H, O and OH on Pt(111) in the presence of implicit water as a function of electrode potential U for different adsorbate coverages.

potentials, i.e., for a more positively charged electrode.

Summarizing the results of this section, the presence of an implicit solvent modifies the adsorption energies of H and on Pt(111) only slightly. This is caused by the small change of the charge density at the Pt electrode induced by the adsorption of these atoms. For a somewhat larger adsorbate such as OH, already a stronger influence of the implicit solvent on the adsorption energy is obtained. The question arises how realistic this effect of the implicit solvent is. In order to address this issue, we introduced an explicit water layer between Pt(111) and the implicit water. The corresponding adsorption energies are discusses in the next section.

TABLE IV. Adsorption enthalpy and adsorption height of H, O and OH on Pt(111) in vacuum calculated using the RPBE-D3 functional at electrode potential U_{SHE}. The changes due to the presence of an implicit solvent are listed in parentheses. The energy ΔH is given in eV and the height h in Ångstrom.

			RPBE-D3	
X		θ_X (ML)	$\Delta H(0)$ (eV)	h (Å)
H	top	1/9	−0.50 (+0.01)	1.56 (+0.00)
		1/3	−0.50 (+0.00)	1.56 (+0.00)
		2/3	−0.47 (−0.01)	1.56 (+0.00)
		1	−0.44 (−0.01)	1.56 (+0.00)
	hcp	1/9	−0.42 (+0.00)	0.90 (+0.00)
	fcc	1/9	−0.47 (+0.00)	0.88 (+0.00)
		1	−0.39 (−0.01)	0.92 (+0.00)
O	top	1/9	2.72 (−0.11)	1.88 (−0.02)
	hcp	1/9	1.96 (−0.02)	1.41 (+0.01)
	fcc	1/9	1.62 (−0.02)	1.33 (+0.00)
		1/3	1.69 (−0.01)	1.36 (+0.01)
		2/3	2.21 (−0.01)	1.32 (+0.01)
		1	2.77 (−0.02)	1.37 (+0.00)
OH	top	1/9	0.83 (−0.12)	2.01 (+0.00)
	hcp	1/9	0.83 (−0.11)	1.74 (−0.02)
	fcc	1/9	0.83 (−0.12)	1.73 (−0.01)
		1/3	0.83 (−0.10)	1.75 (−0.02)
		2/3	0.64 (−0.03)	1.99 (+0.00)

VI. ADSORPTION OF H, O AND OH AT THE Pt(111)/H_2O/IMPLICIT WATER INTERFACE

In order to assess the influence of an explicit water bilayer on the adsorption energy, we consider the adsorption of hydrogen at the energetically most favorable top site. Note that the formation enthalpy in Eq. 8 of a given atomic structure consists of the contributions from hydrogen-Pt bonding, hydrogen-water bilayer interaction and the deformation of the water bilayer. The main difference with metal-vacuum or metal-implicit solvent calculations will stem from the interaction between hydrogen and the water bilayer. The hydrogen-Pt bond length or adsorption height of hydrogen of about 1.5 Å is independent of the H coverage and the presence of implicit and/or explicit water for the stable top adsorption site. However, hydrogen adsorption can result in a strong rearrangement of the explicit water bilayer.

In practice, we define the hydrogen adsorption enthalpy according to Eq. 8 with respect to a Pt slab and a water bilayer. In order to model the Pt electrode-water interface, we select the H-up water bilayer structure (Fig. 2f) which is most stable in the presence of implicit water as the reference configuration, i.e., E_{slab} in Eq. 8 is the total energy of the configuration depicted in Fig. 2f. The number of hydrogen and oxygen atoms (n_H and n_O) to Eq. 8 corresponds to the difference of H and O species with regard to the reference configuration.

In Table V, the enthalpies of hydrogen adsorption in different enviroment are listed as derived from calculations using the PBE, PBE-TS, RPBE-D3 and BEEF functionals. Note that in the presence of the water bilayer, there are three inequivalent surface atoms within the $\sqrt{3} \times \sqrt{3}$ unit cell, as illustrated in Fig. 2e and f.

According to Fig. 4, below $U = 0.5$ V, the Pt(111) electrode is fully covered by hydrogen. The presence of the hydrogen monolayer shifts the water bilayer upward by about 1 Å and reduces metal-water interaction (see Fig. 5), as already found before [50]. Upon this shift, the water bilayer remains in its ice-like structure. AIMD simulations at room temperature have even found that the water bilayer on H-covered Pt(111) is more ordered than the bilayer on clean Pt(111) [50] which has been explained by the stronger water-water interaction due to the weakened electrode-water interaction [3, 50]. Furthermore, the adsorption energy of water on H-covered Pt(111) is almost the same as on clean Pt(111) as the weakened substrate-water interaction is almost exactly compensated by the increased water-water

TABLE V. The adsorption enthalpy of H adsorbate structures on Pt(111) with/without explicit water bilayer in vacuum and in implicit water. The electrode potential is chosen to be $U = 0\,\mathrm{V}$.

PBE	θ_X (ML)	vacuum (eV)	implicit water (eV)
H_{top}	1	−0.41	−0.42
H_{top}/H-down	1	−0.40	−0.36
H_{top}/H-up	1	−0.41	−0.38
H_{top}	1/9	−0.50	−0.50
H_{top1}/H-down	1/9	−0.73	−0.27
H_{top1}/H-up	1/9	−0.48	−0.46
H_{top2}/H-down	1/9	−1.02	−0.56
H_{top2}/H-up	1/9	−0.46	−0.37
H_{top3}/H-down	1/9	−0.77	−0.30
H_{top3}/H-up	1/9	−0.43	−0.31
PBE-TS	θ_X (ML)	vacuum (eV)	implicit water (eV)
H_{top}	1	−0.47	−0.47
H_{top}/H-down	1	−0.44	−0.36
H_{top}/H-up	1	−0.43	−0.41
H_{top}	1/9	−0.55	−0.55
H_{top1}/H-down	1/9	−0.90	−0.30
H_{top1}/H-up	1/9	−0.56	−0.49
H_{top2}/H-down	1/9	−1.30	−0.62
H_{top2}/H-up	1/9	−0.43	−0.38
H_{top3}/H-down	1/9	−0.84	−0.27
H_{top3}/H-up	1/9	−0.90	−0.39
RPBE-D3	θ_X (ML)	vacuum (eV)	implicit water (eV)
H_{top}	1	−0.44	−0.45
H_{top}/H-down	1	−0.38	−0.31
H_{top}/H-up	1	−0.35	−0.33
H_{top}	1/9	−0.50	−0.51
H_{top1}/H-down	1/9	−1.05	−0.36
H_{top1}/H-up	1/9	−0.51	−0.46
H_{top2}/H-down	1/9	−1.10	−0.40
H_{top2}/H-up	1/9	−0.32	−0.25
H_{top3}/H-down	1/9	−0.83	−0.15
H_{top3}/H-up	1/9	−0.29	−0.41
BEEF	θ_X (ML)	vacuum (eV)	implicit water (eV)
H_{top}	1	−0.25	−0.25
H_{top}/H-down	1	−0.23	−0.19
H_{top}/H-up	1	−0.23	−0.22
H_{top}	1/9	−0.32	−0.32
H_{top1}/H-down	1/9	−0.39	−0.18
H_{top1}/H-up	1/9	−0.33	−0.32
H_{top2}/H-down	1/9	−0.65	−0.36
H_{top2}/H-up	1/9	−0.28	−0.36
H_{top3}/H-down	1/9	−0.32	+0.02
H_{top3}/H-up	1/9	−0.49	−0.15

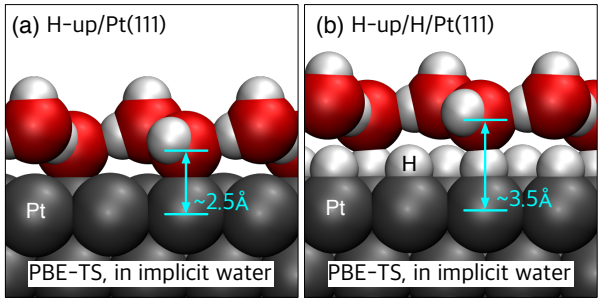

FIG. 5. Sideview of a water bilayer in implicit water (a) without and (b) with a hydrogen monolayer on Pt(111).

interaction [3, 50]. As a consequence, the hydrogen adsorption energy for a monolayer becomes almost independent from the presence of a H-up and H-down water bilayer (see Table V). This is particularly true for the PBE functional, which is characterized by a relative weak water-Pt interaction (E_{ads}), as shown in Table III. The presence of implicit water, however, causes a decrease of the hydrogen adsorption enthalpy by 60 and 40 meV when the H-down and H-up bilayer are introduced, respectively.

When dispersion corrections are included, then the water-Pt interaction becomes stronger, as discussed above. Consequently, in the PBE-TS calculations, the decrease of adsorption enthalpy in the presence of a water bilayer becomes more significant than in the pure PBE case, both in vacuum and in the presence of implicit water. This is also true for the RPBE-D3 calculations. Thus upon taking into account the explicit water bilayer at the interface, the H adsorption enthalpy decreases in general when considering dispersion corrections, because the hydrogen adsorbates destabilizes the water bilayer, as reported in previous studies [67].

For the sake of completeness, we have also studied the influence of the presence of water on hydrogen adsorption energies at a hydrogen coverage of 1/9. Such configurations might also be relevant for electrocatalytic processes. For such a configuration, the water layer is not lifted as there is still a significant water-metal interaction present, and hence there is also a stronger interaction between the explicit water layer and the adsorbed hydrogen. This is particularly true for the H_{top1}/H-down configuration which is associated with a large hydrogen adsorption energy in vacuum. As depicted in Fig. 6a, this energy gain is associated with a strong rearrangement of the water bilayer compared to Fig. 2e, the oxygen atom in a water molecule at the top2 site is lifted up by 1.25 Å. As noted above, the reference here corresponds to the H-up configuration which is less stable than the H-down configuration in vacuum (see Table III). Hence the energy gain upon forming the more favorable H-down water structure within the considered 3×3 surface unit cell also contributes to the H adsorption enthalpy for the H-down

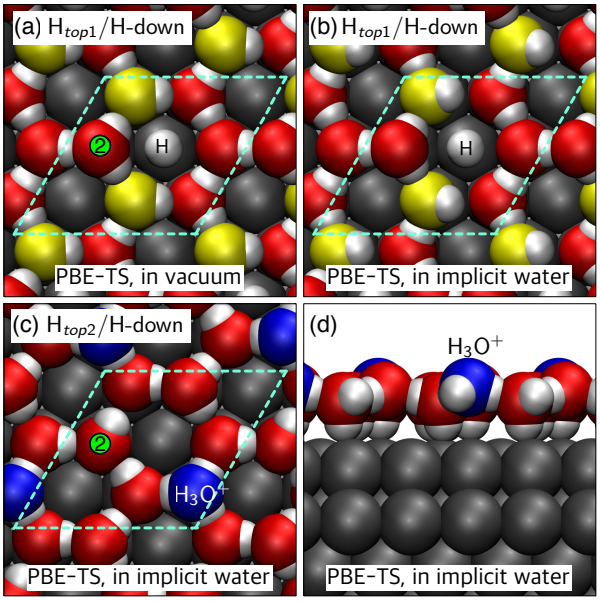

FIG. 6. Top site adsorption of hydrogen with the hydrogen coverage of 1/9 ML (a) at top1 site in vacuum, (b) at top1 site in implicit water and (c) at top2 site in implicit water in the presence of a H-down bilayer. In (d), the side view of (c) is depicted.

water structure. This is no longer the case in implicit water. In fact, the presence of implicit water induces a significant rearrangement of the top1/H-down configuration, as Fig. 6b illustrates. One hydrogen bond of the yellow colored water molecule breaks and the non-bonded OH group turns slightly upward which is the more stable configuration in implicit water. However, the energy cost associated with the bond-breaking renders this configuration rather unfavorable. This severe influence of the presence of implicit water requires further studies with thicker layers of explicit water.

Finally, we discuss proton transfer to the water bilayer leading to the formation of a H_3O^+ molecule [68]. This occurs spontaneously when a hydrogen atom is introduced at the top2 site in the presence of a H-down bilayer as illustrated in Figs. 6c and d. Firstly, the hydronium molecule is created by the transfer of the hydrogen atom originally placed at the top2 site to the water bilayer. The proton then relaxes towards the water molecule highlighted in blue in Figs. 6c and d in a kind of Grotthuss mechanism [69]. The O-H distances of this molecule indicate that it indeed can be considered as a H_3O^+ molecule. The hydronium molecule is rather flat and therefore difficult to accommodate in the bilayer in any other canted configuration. This drives the formation of the H_3O^+ molecule from the original top2 site to the site indicated in Figs. 6c and d. Note that the formation enthalpy for the top2/H-down configuration at coverage 1/9 leading to the formation of the H_3O^+ molecule is the largest both in vacuum and in implicit water for all considered functionals according to Table V. This means that it is energetically favorable to transfer a hydrogen atom to the water layer at low hydrogen concentration. This mechanism, however, requires the presence of an explicit water bilayer as the transfer cannot be described using only implicit water.

VII. CONCLUSIONS

In this work, we have studied the performance of a computationally efficient implicit water scheme in the modeling of electrochemical metal/electrolyte interfaces. First, we have calculated the standard electrode potential of half cell reactions by combining the computational hydrogen electrode with an implicit solvation model. The computational results are in satisfactory agreement with experimental values. Thus, the combination of these methods represents a simple and efficient technique to derive standard electrode potentials within a conventional DFT framework.

Secondly, we have tested various density functionals and van der Waals correction schemes to describe the Pt(111)-water and water-water interactions. We find that the pairwise vdW-D correction schemes PBE-D3, PBE-TS, RPBE-D3 yield similar results with respect to the water-metal interaction. However, the dispersion corrections do not correct the overstructuring of PBE liquid water, whereas RPBE-D3 reproduces also liquid water properties well, as found in previous studies [11].

Thirdly, we have contrasted Pt(111) electrode properties in the presence of vacuum, an explicit water layer, implicit water, and the combination of an explicit water layer with implicit water. The inclusion of implicit water modifies the adsorption energies of H, O and OH to a rather small extent. However, for the PBE-derived functionals, the H-down layer becomes unstable in the presence of implicit water. These findings call for further testing with thicker layers of explicit water. Our results show that it is necessary to take water into account in the modeling of electrochemical processes at the interface between a metal electrolyte and an aqueous electrolyte. The description of processes such as the proton transfer into the water leading to the formation of a H_3O^+ ion at the interface requires the inclusion of an explicit water layer. Here the combination of a few explicit water layers with an implicit water model represents a computational attractive method for a more realistic first-principles treatment of electrochemical interfaces with aqueous electrolytes.

ACKNOWLEDGEMENT

This research has been supported by the German Science Foundation (DFG) through the research unit FOR 1376 (DFG contract GR 1503/21-1) and by the Baden-Württemberg Foundation within the Network of Excel-

lence Functional Nanostructures. Computer time has been provided by the BW-Grid and the BW-Uni-Cluster projects of the federal state of Baden-Württemberg. The work at the University of Florida was supported by the National Science Foundation under CAREER award No. DMR-1056587

[1] W. Schmickler, Chemical Reviews **96**, 3177 (1996), PMID: 11848857.

[2] R. Guidelli and W. Schmickler, Electrochimica Acta **45**, 2317 (2000).

[3] A. Groß, F. Gossenberger, X. Lin, M. Naderian, S. Sakong, and T. Roman, J. Electrochem. Soc. **161**, E3015 (2014).

[4] N. G. Hörmann, M. Jäckle, F. Gossenberger, T. Roman, K. Forster-Tonigold, M. Naderian, S. Sakong, and A. Groß, J. Power Sources **275**, 531 (2015).

[5] J. K. Norskov, T. Bligaard, J. Rossmeisl, and C. H. Christensen, Nat Chem **1**, 37 (2009).

[6] S. Schnur and A. Groß, Catal. Today **165**, 129 (2011).

[7] F. Calle-Vallejo and M. T. Koper, Electrochim. Acta **84**, 3 (2012).

[8] K. Tonigold and A. Groß, J. Comp. Chem. **33**, 695 (2012).

[9] F. Buchner, K. Forster-Tonigold, B. Uhl, D. Alwast, N. Wagner, H. Farkhondeh, A. Groß, and R. J. Behm, ACS Nano **7**, 7773 (2013).

[10] J. Klimeš, D. R. Bowler, and A. Michaelides, J. Phys.: Condens. Matter **22**, 022201 (2010).

[11] K. Forster-Tonigold and A. Groß, J. Chem. Phys. **141**, 064501 (2014).

[12] J. K. Nørskov, J. Rossmeisl, A. Logadottir, L. Lindqvist, J. R. Kitchin, T. Bligaard, and H. Jónsson, J. Phys. Chem. B **108**, 17886 (2004).

[13] G. S. Karlberg, J. Rossmeisl, and J. K. Norskov, Phys. Chem. Chem. Phys. **9**, 5158 (2007).

[14] E. Skulason, G. S. Karlberg, J. Rossmeisl, T. Bligaard, J. Greeley, H. Jonsson, and J. K. Norskov, Phys. Chem. Chem. Phys. **9**, 3241 (2007).

[15] J. Rossmeisl, E. Skúlason, M. E. Björketun, V. Tripkovic, and J. K. Nørskov, Chemical Physics Letters **466**, 68 (2008).

[16] V. Tripkovic, M. E. Björketun, E. Skúlason, and J. Rossmeisl, Phys. Rev. B **84**, 115452 (2011).

[17] K. Letchworth-Weaver and T. A. Arias, Phys. Rev. B **86**, 075140 (2012).

[18] J. Lischner and T. A. Arias, J. Phys. Chem. B **114**, 1946 (2010).

[19] S. A. Petrosyan, A. A. Rigos, and T. A. Arias, J. Phys. Chem. B **109**, 15436 (2005).

[20] S. A. Petrosyan, J.-F. Briere, D. Roundy, and T. A. Arias, Phys. Rev. B **75**, 205105 (2007).

[21] R. Sundararaman, K. Letchworth-Weaver, and T. A. Arias, J. Chem. Phys. **137**, 044107 (2012).

[22] D. Gunceler, K. Letchworth-Weaver, R. Sundararaman, K. A. Schwarz, and T. A. Arias, Modelling Simul. Mater. Sci. Eng. **21**, 074005 (2013).

[23] M. Fishman, H. L. Zhuang, K. Mathew, W. Dirschka, and R. G. Hennig, Phys. Rev. B **87**, 245402 (2013).

[24] K. Mathew, R. Sundararaman, K. Letchworth-Weaver, T. A. Arias, and R. G. Hennig, J. Chem. Phys. **140**, 084106 (2014).

[25] S. Grimme, J. Antony, S. Ehrlich, and H. Krieg, J. Chem. Phys. **132**, 154104 (2010).

[26] A. Tkatchenko and M. Scheffler, Phys. Rev. Lett. **102**, 073005 (2009).

[27] H. Ogasawara, B. Brena, D. Nordlund, M. Nyberg, A. Pelmenschikov, L. G. M. Pettersson, and A. Nilsson, Phys. Rev. Lett. **89**, 276102 (2002).

[28] A. Hodgson and S. Haq, Surf. Sci. Rep. **64**, 381 (2009).

[29] S. Schnur and A. Groß, New J. Phys. **11**, 125003 (2009).

[30] M. Faheem and A. Heyden, J. Chem. Theor. Comp. **10**, 3354 (2014).

[31] J.-L. Fattebert and F. Gygi, J. Comp. Chem. **23**, 662 (2002).

[32] J.-L. Fattebert and F. Gygi, Int. J. Quant. Chem. **93**, 139 (2003).

[33] O. Andreussi, I. Dabo, and N. Marzari, J. Chem. Phys. **136**, 064102 (2012).

[34] J. Harl and G. Kresse, Phys. Rev. B **77**, 045136 (2008).

[35] S. Grimme, Wiley Interdisciplinary Reviews: Computational Molecular Science **1**, 211 (2011).

[36] M. Dion, H. Rydberg, E. Schröder, D. C. Langreth, and B. I. Lundqvist, Phys. Rev. Lett. **92**, 246401 (2004).

[37] J. Wellendorff, K. T. Lundgaard, A. Møgelhøj, V. Petzold, D. D. Landis, J. K. Nørskov, T. Bligaard, and K. W. Jacobsen, Phys. Rev. B **85**, 235149 (2012).

[38] W. A. Donald, R. D. Leib, J. T. O'Brien, M. F. Bush, and E. R. Williams, J. Am. Chem. Soc. **130**, 3371 (2008).

[39] A. A. Isse and A. Gennaro, J. Phys. Chem. B **114**, 7894 (2010).

[40] G. Kresse and J. Furthmüller, Phys. Rev. B **54**, 11169 (1996).

[41] P. E. Blöchl, Phys. Rev. B **50**, 17953 (1994).

[42] J. P. Perdew, K. Burke, and M. Ernzerhof, Phys. Rev. Lett. **77**, 3865 (1996).

[43] J. Klimeš, D. R. Bowler, and A. Michaelides, Phys. Rev. B **83**, 195131 (2011).

[44] NIST Computational Chemistry Comparison and Benchmark Database NIST Standard Reference Database Number 101 Release 16a, August 2013, Editor: Russell D. Johnson III, http://cccbdb.nist.gov/.

[45] S. G. Bratsch, J. Phys. Chem. Ref. Data **18**, 1 (1989).

[46] W. Greiner, L. Neise, and H. Stöcker, *Thermodynamik und Statistische Mechanik*, Harri Deutsch, Frankfurt am Main, 1987.

[47] M. W. Chase Jr., NIST-JANAF Thermochemical Tables, Fourth Edition, J. Phys. Chem. Ref. Data, Monograph 9, 1988.

[48] A. BenNaim and Y. Marcus, The Journal of Chemical Physics **81**, 2016 (1984).

[49] W. Haynes, *CRC Handbook of Chemistry and Physics, 95th Edition*, CRC Press, 2015.

[50] T. Roman and A. Groß, Catalysis Today **202**, 183 (2013).

[51] A. Roudgar and A. Groß, Chem. Phys. Lett. **409**, 157 (2005).

[52] P. Jurecka, J. Sponer, J. Cerny, and P. Hobza, Phys. Chem. Chem. Phys. **8**, 1985 (2006).

[53] M. V. Fernández-Serra and E. Artacho, J. Chem. Phys. **121**, 11136 (2004).
[54] J. VandeVondele, F. Mohamed, M. Krack, J. Hutter, M. Sprik, and M. Parrinello, J. Chem. Phys. **122**, 014515 (2005).
[55] L.-M. Liu, M. Krack, and A. Michaelides, J. Chem. Phys. **130**, 234702 (2009).
[56] S. Meng, E. G. Wang, and S. Gao, Phys. Rev. B **69**, 195404 (2004).
[57] A. Michaelides, Appl. Phys. A **85**, 415 (2006).
[58] H. Ogasawara, J. Yoshinobu, and M. Kawai, J. Chem. Phys. **111**, 7003 (1999).
[59] J. Carrasco, A. Hodgson, and A. Michaelides, Nat Mater **11**, 667 (2012).
[60] K. Motobayashi, L. Árnadóttir, C. Matsumoto, E. M. Stuve, H. Jónsson, Y. Kim, and M. Kawai, ACS Nano **8**, 11583 (2014).
[61] L. Firment and G. Somorjai, Surf. Sci. **84**, 275 (1979).
[62] C. Panja, N. Saliba, and B. E. Koel, Surf. Sci. **395**, 248 (1998).
[63] W. Lew, M. C. Crowe, E. Karp, and C. T. Campbell, J. Phys. Chem. C **115**, 9164 (2011).
[64] S. C. Badescu, P. Salo, T. Ala-Nissila, S. C. Ying, K. Jacobi, Y. Wang, K. Bedürftig, and G. Ertl, Phys. Rev. Lett. **88**, 136101 (2002).
[65] P. Ferrin, S. Kandoi, A. U. Nilekar, and M. Mavrikakis, Surf. Sci. **606**, 679 (2012).
[66] B. Genorio, D. Strmcnik, R. Subbaraman, D. Tripkovic, G. Karapetrov, V. R. Stamenkovic, S. Pejovnik, and N. M. Marković, Nat. Mater. **9**, 998 (2010).
[67] A. Roudgar and A. Groß, Surf. Sci. **597**, 42 (2005).
[68] P. Quaino, N. Luque, G. Soldano, R. Nazmutdinov, E. Santos, T. Roman, A. Lundin, A. Groß, and W. Schmickler, Electrochim. Acta **105**, 248 (2013).
[69] D. Marx, ChemPhysChem **7**, 1848 (2006).